Table IV. Intrinsic Barriers of Symmetric Reactions. Integrated Charge on X in CH_3X, and Basicity of X^- in the Gas Phase and in Solution[a]

X	$\Delta E^{\ddagger}_{0(XX)}$[b] (kJ/mol)	$-Q_X$ (e)	pK_a	ΔH (kJ/mol)
H	235.15	-0.066	35	1676
CCH	213.82	0.290	24	1572
*C*N	191.02	0.328	9.21	1478
*N*C	130.24	0.650		
PH_2	147.67	-0.515	29	1551
SH	110.83	-0.003	7.0	1480
Cl	75.44	0.224	-6 to -7	1395
NH_2	145.30	0.350	32.5	1673
OH	98.49	0.545	15.7	1636
OOH	76.35	0.604	11.6[c]	
F	52.70	0.626	3.18	1555

[a] The pK_a and ΔH values are from ref 25a and 25b, respectively. ΔH is the enthalpy change of the reaction $HX \rightarrow H^+ + X^-$ in the gas phase at 298 K. [b] In kJ/mol to be consistent with the units of ΔH. [c] Data from ref 25c.

group to which the reaction belongs (ω value) and the electronegativity of X (τ value). The classification that we used is based on the relationship between $\Delta E^{\ddagger}_0$ and ΔE°_c. At first, it seems that our ω factor is similar to Shaik and Pross's *f* factor, and our τ factor is similar to their $(I_{N:} - A_{RX})$ factor. However, quite different results were obtained from the two analyses. For example, according to their calculations,[5] CCH and OH have similar *f* factors ($W_{R:} = 0.36$), F and Cl have similar *f* factors ($W_{R:} \sim 0.24$-0.25), and $W_{R:} = 0.30$ for *C*N, whereas according to our analysis, CCH and *C*N belong to one group and OH and F belong to another group. Moreover, according to the Shaik and Pross model, the $\Delta E^{\ddagger}_0$ value for the symmetric reaction N = X = F is larger than that of the reaction N = X = Cl because the former has a larger energy gap factor ($I_{N:} - A_{RX}$). According to our model, there are two competing factors: the electronic structure factor (ω value) favors N = X = Cl, since it involves an excess ψ_3 contribution to the TS; however, the electronegativity factor (τ value) favors N = X = F. Depending on which factor dominates, the intrinsic barrier for F may be smaller or larger than that of Cl. Results obtained at the HF level[7a-c,23] show that the N = X = Cl case has a smaller intrinsic barrier. However, results obtained at the MP2′ and MP2 levels[7b,c] indicate that the N = X = F case has a smaller intrinsic barrier in agreement with recent configuration interaction calculations.[24]

Within each group, the intrinsic barrier $\Delta E^{\ddagger}_{0(XX)}$ is related to the charge (Q_X) on X in CH_3X (see Table IV). As discussed above, $\Delta E^{\ddagger}_{0(XX)}$ is related to the electronegativity of X within each group. Since Q_X is a measure of the electronegativity of X, the relationship between $\Delta E^{\ddagger}_{0(XX)}$ and Q_X is not unexpected. Furthermore, within each group the intrinsic barrier is related to the base strength of X^- (see pK_a values in Table IV). As the base strength increases (pK_a increases), the intrinsic barrier increases. This can be understood by the fact that the base strength of X^- reflects the electron-donating ability of X^-. It is an indication of the electronegativity of X as well.

Conclusions

Chemical reactions are classified according to molecular and mechanistic criteria. In the case of the S_N2 reactions discussed in this paper, the reactions can be classified according to the hybridization of the leaving group (specifically, the atom adjacent to carbon) and the electronic structure of the TS. A sp-hybridized atom results in a rapid ascent or a large curvature of the reactant energy profile and a high intrinsic barrier. An excess contribution of ψ_3 to the TS in eq 7 lowers the intrinsic barrier. Within each group, the intrinsic barrier is related to the electronegativity of the leaving group. As the electronegativity of the leaving group increases, the intrinsic barrier decreases. Within each group there is a linear relationship between $\Delta E^{\ddagger}$ and ΔE°_c.

Acknowledgment. A Killam postgraduate scholarship (to Z.S.) from Dalhousie University and the financial assistance of the Natural Sciences and Engineering Research Council of Canada in the form of an operating grant (to R.J.B.) are gratefully acknowledged. We thank Dalhousie University Computing and Information Services for a generous allocation of computer time. We also thank Dr. R. Vetter for sending us a preprint.

(23) Wolfe, S.; Mitchell, D. J.; Schlegel, H. B. *J. Am. Chem. Soc.* **1981**, *103*, 7694.

(24) Vetter, R.; Zülicke, L. *J. Am. Chem. Soc.* **1990**, *112*, 5136.

(25) (a) Reference 22, p 294, 297. (b) Bartmess, J. E.; Scott, J. A.; McIver, R. T., Jr. *J. Am. Chem. Soc.* **1979**, *101*, 6046. (c) Weast, R. C.; Lide, D. R.; Astle, M. J.; Beyer, W. H. *CRC Handbook of Chemistry and Physics*, 70th ed.; CRC Press: Boca Raton, FL, 1989, p D-165.

The Fluorophosphoranyl Series: Theoretical Insights into Relative Stabilities and Localization of Spin

Christopher J. Cramer

Contribution from the U.S. Army Chemical Research Development and Engineering Center, Research Directorate, Physics Division, Chemometric and Biometric Modeling Branch, Aberdeen Proving Ground, Maryland 21010-5423. *Received May 9, 1990*

Abstract: The nine isomeric local minima within the complete fluorophosphoranyl series ($H_nPF_{4-n}^{\bullet}$, $n = 0$-4) have been investigated at the UHF/6-31G* and higher levels. Quantitative analysis of fluorine apicophilicity and hyperconjugative effects within the trigonal-bipyramidal series is presented. The ability of atomic orbitals on axially disposed fluorine atoms to participate in either a hyperconjugative donor or acceptor role is quite limited in comparison to analogous opportunities for equatorially disposed fluorine atoms. Decomposition of metathesis energy changes into apicophilic and hyperconjugative components permits rational evaluation of the corresponding equilibria. Localization of spin density is accomplished efficiently by using the calculated MP2/6-311G** electron density. Fermi contact integrals derived therefrom allow for highly accurate prediction of isotropic hyperfine coupling constants after application of a small scaling factor. Techniques alternatively using s-orbital spin density for such predictions are far less satisfactory.

Phosphoranyl radicals, first proposed as metastable reaction intermediates in 1957,[1] have been the subject of detailed study. Implicated, inter alia, as playing a role in radiolytically damaged nucleic acid polymers, they have attracted considerable experi-

Table I. Absolute and Relative Energies for 1–5 Calculated by Using UHF/6-31G* Geometries

	energy[a]					
compd	UHF/6-31G*	UHF/6-311G**	MP2(FC)/ 6-311G**	MP3(FC)/ 6-311G**	MP4(FC)/ 6-311G**	MP2/6-311G**
1	−342.9366	−342.9700	−343.1150	−343.1395	**−343.1472**	−343.2393
2a[b]	−441.8335	−441.8911	−442.2302	−442.2443	**−442.2612**	−442.3731
2b	−441.8211	−441.8769	−442.2153	−442.2301	**−442.2466**	−442.3583
	7.8	*8.9*	*9.3*	*8.9*	***9.2***	*9.3*
3a[b]	−540.7367	−540.8158	−541.3494	−541.3527	**−541.3792**	−541.5111
3b	−540.7237	−540.8013	−541.3345	−541.3389	**−541.3649**	−541.4962
	8.2	*9.1*	*9.3*	*8.7*	***9.0***	*9.3*
3c	−540.7183	−540.7957	−541.3292	−541.3335	**−541.3596**	−541.4909
	11.5	*12.6*	*12.7*	*12.1*	***12.3***	*12.6*
4a[b]	−639.6322	−639.7293	−640.4589	−640.4523	**−640.4880**	−640.6393
4b	−639.6269	−639.7240	−640.4535	−640.4477	**−640.4831**	−640.6341
	3.3	*3.3*	*3.4*	*2.9*	***3.1***	*3.3*
5	−738.5336	−738.6482	−739.5744	−739.5585	**−739.6028**	−739.7735

[a] Absolute energies in hartrees; relative energies (italics) in kilocalories per mole. [b] Relative energy is 0.0 at all levels.

Chart I

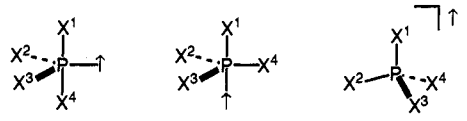

TBP_e TBP_a DT

mental interest.[2] Spectroscopists have also shown interest in phosphoranyl radicals due to their intriguing stereochemistry: they usually adopt a trigonal-bipyramidal geometry where the unpaired electron acts as a fifth "substituent", which is preferentially localized equatorially—a so-called TBP_e structure (Chart I).[3] In 1976, Howell and Olsen[4] provided the first thorough, ab initio study of both the electronic structure and the conformational hypersurface for the simplest phosphoranyl radical, $PH_4^•$ (**1**). While noting that their results should be viewed with some caution, since with the employed 4-31G basis set the experimentally known **1** was determined to be unstable to dissociation, they were able to provide detailed insights into the possible pseudorotational pathways available to **1** and proposed a second-order Jahn–Teller effect as giving rise to the observed TBP_e geometry. They also provided[4] the first ab initio data on the series of fluorophosphoranyls[5] $H_3PF^•$ (**2**), $H_2PF_2^•$ (**3**), $HPF_3^•$ (**4**), and $PF_4^•$ (**5**). Employing the predicted s-orbital spin density to calculate isotropic hyperfine coupling (hfs) constants,[6] they were able to qualitatively reproduce the trends in the spectroscopic data[7] from **1**, **2**, **4**, and **5**. Quantitative agreement was poor, however, reflecting the low levels of theory to which they were constrained at the time by the size of the molecules.

Janssen et al.[8] provided additional data for **1**, **2**, **4**, and **5** with the molecules constrained to geometries of C_{3v} symmetry. This constraint resulted in the unpaired electron localizing apically in the trigonal bipyramid (TBP_a). Their primary contribution was to show that in the case of forced C_{3v} symmetry this type of structure is preferred over the alternative distorted tetrahedron (DT), where the unpaired electron is primarily localized in the σ^*_{P-X} orbital of the quasi-apical bond (Chart I). Such DT structures have been proposed by various authors[5e,9] for phosphoranyl radicals shown by ESR to genuinely adopt C_{3v} geometries.[9d,10] The difference between the two is subtle, especially when the bond angle between the "apical" and "equatorial" substituents is somewhere between the ideal extremes of 90° and 109.5° expected for the TBP_a and DT structures, respectively. While ESR evaluation of the degree of spin density at phosphorus can provide some assistance in differentiation, the assignment is in general still subject to interpretation, especially given the paucity of high-level theoretical correlations between structure and spectroscopy for phosphoranyl systems.[11a]

These same authors did predict hfs constants based on valence orbital spin densities, employing the same moderate level of theory as Howell and Olsen. However, since these geometries *do not correspond to local minima*, comparison to experiment was not possible.

Our own interest in phosphoranyl radicals[11] arises from their inferred intermediacy in the biodegradation of certain environmentally toxic organophosphonates.[12] We are particularly intrigued by conformational processes that permute substituent locations and those factors that determine the geometry (TBP_a, TBP_e, or DT) a given phosphoranyl radical will adopt. There remains significant controversy in the literature today over the

(1) Ramirez, F.; McElvie, N. *J. Am. Chem. Soc.* **1957**, *79*, 5929.

(2) (a) Aagaard, O. M.; Janssen, R. A. J.; de Waal, B. F. M.; Buck, H. M. *J. Am. Chem. Soc.* **1990**, *112*, 938. For more general reviews, see: (b) Bentrude, W. G. *Acc. Chem. Res.* **1982**, *15*, 117. (c) Roberts, B. P. In *Advances in Free Radical Chemistry*; Williams, G. H., Ed.; Heyden and Sons: London, 1980; Vol. 6, p 225.

(3) For reviews and compilations of data, see: (a) Tordo, P. *Landolt-Börnstein, New Series*; Springer-Verlag: Berlin, 1988; Vol. II, 17/e, p 254. (b) Schipper, P.; Janssen, E. H. J. M.; Buck, H. M. *Top. Phosphorus Chem.* **1977**, *9*, 407. For some specific radicals, see the following. (c) PH_4: Colussi, A. J.; Morton, J. R.; Preston, K. F. *J. Chem. Phys.* **1975**, *62*, 2004. (d) PF_4: Fessenden, R. W.; Schuler, R. H. *J. Chem. Phys.* **1966**, *45*, 1845. (e) PCl_4: Kokoszka, G. F.; Brinkman, F. E. *J. Am. Chem. Soc.* **1970**, *92*, 1199. (f) $POCl_3^-$: Gilibro, T.; Williams, F. *J. Am. Chem. Soc.* **1974**, *96*, 6032. (g) $ROPH_3$: Krusic, P. J.; Mahler, W.; Kochi, J. K. *J. Am. Chem. Soc.* **1972**, *94*, 6033. (h) $(RO)Cl_2PO^-$: Nelson, D. J.; Symons, M. C. R. *J. Chem. Soc., Dalton Trans.* **1974**, 1164. (i) $(H_3PCHC(O)H)^-$: Geoffroy, M.; Rao, G.; Tancic, Z.; Bernardinelli, G. *J. Am. Chem. Soc.* **1990**, *112*, 2826.

(4) Howell, J. M.; Olsen, J. F. *J. Am. Chem. Soc.* **1976**, *98*, 7119.

(5) These species have also been studied at semiempirical levels. (a) Colussi, A. J.; Morton, J. R.; Preston, K. F. *J. Phys. Chem.* **1975**, *79*, 651. (b) Higuchi, J. *J. Chem. Phys.* **1969**, *50*, 1001. (c) Bischof, P.; Friedrich, G. *J. Comput. Chem.* **1982**, *3*, 486. (d) VanDijk, J. M. I.; Pennings, J. F. M.; Buck, H. M. *J. Am. Chem. Soc.* **1975**, *97*, 4836. (e) Penkovskii, V. V. *Dokl. Akad. Nauk. SSSR* **1978**, *243*, 375. (f) Weber, J.; Geoffrey, M. *Theor. Chim. Acta* **1977**, *43*, 299.

(6) Froese, C. *J. Chem. Phys.* **1968**, *48*, 1417.

(7) (a) Colussi, A. J.; Morton, J. R.; Preston, K. F. *J. Phys. Chem.* **1975**, *79*, 1855. (b) Fessenden, R. W. *J. Magn. Reson.* **1969**, *1*, 277. (c) Nelson, W.; Jackel, G.; Gordy, W. *J. Chem. Phys.* **1970**, *52*, 4572. See also: References 3c and 3d.

(8) Janssen, R. A. J.; Visser, G. J.; Buck, H. M. *J. Am. Chem. Soc.* **1984**, *106*, 3429.

(9) (a) Giles, J. R. M.; Roberts, B. P. *J. Chem. Soc., Perkin Trans. 2* **1981**, 1211. (b) Evans, J. C.; Mishra, S. P. *J. Inorg. Nucl. Chem.* **1981**, *43*, 481. (c) Baban, J. A.; Roberts, B. P. *J. Chem. Soc., Chem. Commun.* **1979**, 537. (d) Symons, M. C. R. *Chem. Phys. Lett.* **1976**, *40*, 226.

(10) Hay, R. S.; Roberts, B. P.; Singh, K.; Wilkinson, J. P. T. *J. Chem. Soc., Perkin Trans. 2* **1979**, 756. (b) Baban, J. A.; Cooksey, C. J.; Roberts, B. P. *J. Chem. Soc., Perkin Trans. 2* **1979**, 781. (c) Boekestein, G.; Janssen, E. H. J. M.; Buck, H. M. *J. Chem. Soc., Chem. Commun.* **1974**, 118. (d) Berclaz, T.; Geoffroy, M.; Lucken, E. A. C. *Chem. Phys. Lett.* **1975**, *36*, 677. (e) Cattani-Lorente, M.; Bernardinelli, G.; Geoffroy, M. *Helv. Chim. Acta* **1987**, *70*, 1897. (f) Janssen, R. A. J.; Sonnemans, M. H. W.; Buck, H. M. *J. Am. Chem. Soc.* **1986**, *108*, 6145.

(11) (a) Cramer, C. J. *J. Am. Chem. Soc.* **1990**, *112*, 7965. (b) Cramer, C. J.; Famini, G. R. *J. Am. Chem. Soc.* **1990**, *112*, 5460. (c) Cramer, C. J.; Famini, G. R. *Chem. Phys. Lett.* **1990**, *169*, 405.

(12) Loo, S. H.; Peters, N. K.; Frost, J. W. *Biochem. Biophys. Res. Commun.* **1987**, *148*, 148. (b) Avila, L. Z.; Loo, S. H.; Frost, J. W. *J. Am. Chem. Soc.* **1987**, *109*, 6758. (c) Frost, J. W.; Loo, S.; Cordeiro, M. L.; Li, D. *J. Am. Chem. Soc.* **1987**, *109*, 2166. (d) Cordeiro, M. L.; Pompliano, D. L.; Frost, J. W. *J. Am. Chem. Soc.* **1986**, *108*, 332.

Table II. Absolute and Relative Energies for Selected Isomers of **1–5** Calculated by Using UMP2/6-31G* Geometries

	energy[a]			
compd	UHF/ 6-31G*	UMP2/ 6-31G*	UHF/ 6-311G**	UMP2/ 6-311G**
1	−342.9364	−343.0534	−342.9699	−343.2392
2a	−441.8329	−442.1239	−441.8908	−442.3734
3a	−540.7358	−541.2018	−540.8152	−541.5116
4a	−639.6305	−640.2737	−639.7275	−640.6402
	0.0	*0.0*	*0.0*	*0.0*
4b	−639.6250	−640.2683	−639.7217	−640.6347
	3.5	*3.4*	*3.6*	*3.5*
5	−738.5309	−739.3518	−738.6447	−739.7749

[a] Absolute energies in hartrees; relative energies (italics) in kilocalories per mole.

validity of assigning a TBP_a geometry to certain phosphoranyl radicals,[13] with theory well suited to evaluation of the endogenous arguments.[5e,9,14] In addition, this series of molecules provides ample opportunity to examine the role hyperconjugation plays in their structures and stabilities. Such effects are likely to be operative in TBP closed-shell phosphoranes as well. Finally, modern computational methodology allows for a far more accurate orbital partitioning of spin density than that available to earlier investigators. Techniques providing *quantitative* correlation with ESR spectroscopy would be invaluable to settling certain questions of geometry in phosphoranyl radicals. We present here a high-level theoretical treatment of the nine TBP_e local minima available to the complete fluorophosphoranyl series, assess the factors governing structures and energetic equilibria, compare various techniques for predicting hfs constants to the comparative wealth of available spectroscopic data, and predict data for the as yet experimentally unobserved **3**.

Computational Methods

Structures **1–5** were fully optimized at the UHF/6-31G* level[15] of theory. For all of these species, spin contamination was negligible, with expectation values for $\langle S^2 \rangle$ ranging from 0.75 to 0.77. Structures **1**, **2a**, **3a**, **4a**, **4b**, and **5** were in addition fully optimized at the UMP2/6-31G* level with excitation from the core orbitals permitted. Single-point calculations at the UHF, UMP2, UMP3, and UMP4 levels[16] were performed with the 6-311G** basis set[17] with core orbitals frozen (FC) to substitution in the latter two instances, and with both core orbitals frozen and core orbitals left open in the UMP2 case. For the isomeric global minima **1**, **2a**, **3a**, **4a**, and **5**, orbital spin densities and the Fermi contact values derived therefrom were calculated both at the usual SCF level (6-311G**) and at the Z-vector-derived[18] UMP2/6-311G** level. Derivation of hfs constants is described in the text. All calculations were performed with the Gaussian 88 package[19] running on an Ardent Titan.

Results

The nine possible TBP_e local minima for the fluorophosphoranyl series are the isomerically unique C_{2v} **1** and **5**, the C_{2v} **3a** and **3c**, where the two fluorine atoms occupy both apical and both equatorial positions, respectively, the C_s **2a**, **2b**, **4a**, and **4b**, where the unique fluorine (**2**) or hydrogen (**4**) atom occupies either an axial or equatorial site, and finally the C_1 **3b**, which has each of the two unique atom types filling half of each of the two unique pairs of positions (Figure 1). Relaxation of TBP_a structures optimized under the constraints of C_{3v} symmetry (or "pseudo-C_{3v}" symmetry in the cases of **2b**, **3**, and **4**) led smoothly to structures **1–5**; i.e., no TBP_a local minima exist within the series. Structural data for **1–5** are collected in Figure 1 and both absolute and relative (within an isomeric series) energies are presented in Table I. Energies for the five isomeric global minima and also **4b** optimized at the UMP2/6-31G* level may be found in Table II.

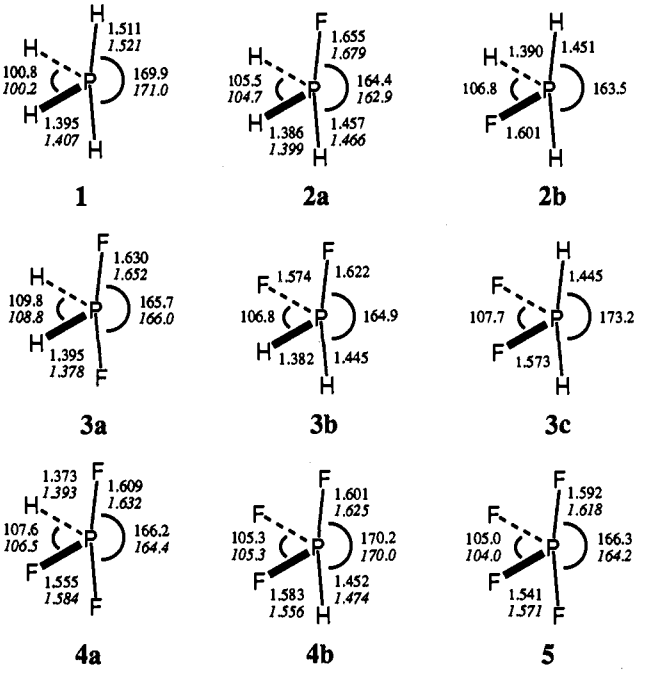

Figure 1. Optimized structural parameters for the fluorophosphoranyl series at the UHF/6-31G* level. Where calculated, UMP2/6-31G* parameters are provided in italics. Bond lengths are in angstroms and bond angles in degrees.

Referring to Figure 1, it is noteworthy that relatively small structural reorganization occurs upon reoptimization at the UMP2/6-31G* level. Bond angle changes are on the order of 1° and bond length changes are only slightly more profound, with lengthening on the order of 0.01–0.03 Å observed. On the other hand, both of these levels predict apical bond lengths shorter than those found at the 4-31G level[4] by up to 0.13 Å. This provides yet another example of the importance of basis set d functions in accurately predicting molecular geometry in expanded valence phosphorus compounds[20] and probably accounts for Howell and Olsen's observation of spontaneous P–H bond homolysis upon relaxation of C_{2v} symmetry.

Equally in accord with literature precedent[21] is the observation that while the fully polarized, valence-triple-ζ 6-311G** basis set affords little improvement in electronic energy over the heavy-atom-polarized, valence-double-ζ 6-31G*, the second-order correlation energy, E(UMP2) − E(UHF), increases considerably with the larger basis set (Table II). In addition, for all but **1**, the common oscillatory nature of the electronic energy with increasing orders of Møller–Plesset correction is observed.

It is further interesting to note the progressive contraction of the P–F bonds with increasing fluorine substitution. In a comprehensive study of singlet AH_mF_n systems, Schleyer and Reed[22]

(13) (a) Hamerlinck, J. H. H.; Schipper, P.; Buck, H. M. *J. Am. Chem. Soc.* **1983**, *105*, 385. (b) Hamerlinck, J. H. H.; Schipper, P.; Buck, H. M. *J. Am. Chem. Soc.* **1980**, *102*, 5679. (c) Hamerlinck, J. H. H.; Schipper, P.; Buck, H. M. *J. Org. Chem.* **1983**, *48*, 306. (d) Hamerlinck, J. H. H.; Schipper, P.; Buck, H. M. *J. Chem. Phys.* **1982**, *76*, 2161.

(14) Roberts, B. P. *Tetrahedron Lett.* **1983**, *3377*.

(15) Francl, M. M.; Pietro, W. J.; Hehre, W. J.; Binkley, J. S.; Gordon, M. S.; DeFrees, D. J.; Pople, J. A. *J. Chem. Phys.* **1982**, *77*, 3654.

(16) MP2: (a) Møller, C.; Plesset, M. S. *Phys. Rev.* **1934**, *46*, 618. MP3(SDT): (b) Pople, J. A.; Seeger, R.; Krishnan, R. *Int. J. Quantum Chem. Symp.* **1977**, *11*, 149. MP4(SDTQ): (c) Krishnan, R.; Pople, J. A. *Int. J. Quantum Chem.* **1978**, *14*, 91. (d) Krishnan, R.; Frisch, M. J.; Pople, J. A. *J. Chem. Phys.* **1980**, *72*, 4244.

(17) (a) Krishnan, R.; Binkley, J. S.; Seeger, R.; Pople, J. A. *J. Chem. Phys.* **1980**, *72*, 650. (b) McLean, A. D.; Chandler, G. S. *J. Chem. Phys.* **1980**, *72*, 5629. (c) Frisch, M. J.; Pople, J. A.; Binkley, J. S. *J. Chem. Phys.* **1984**, *80*, 3265.

(18) Handy, N. C.; Schaeffer, H. F., III *J. Chem. Phys.* **1984**, *81*, 5031.

(19) Frisch, M. J.; Head-Gordon, M.; Schlegel, H. B.; Raghavachari, K.; Binkley, J. S.; Gonzalez, C.; DeFrees, D. J.; Fox, D. J.; Whiteside, R. A.; Seeger, R.; Melius, C. F.; Baker, J.; Martin, R. L.; Kahn, L. R.; Stewart, J. J. P.; Fluder, E. M.; Topiol, S.; Pople, J. A. *Gaussian 88*; Gaussian Inc.: Pittsburgh, PA, 1988.

(20) For a thorough comparison of the relative performances of polarized and unpolarized basis sets in hypervalent molecules, see: Reference 21b, pp 181–186.

(21) (a) Dykstra, C. E. *Ab Initio Calculation of the Structures and Properties of Molecules*; Elsevier: Amsterdam, 1988. (b) Hehre, W. J.; Radom, L.; Schleyer, P. v. R.; Pople, J. A. *Ab Initio Molecular Orbital Theory*; Wiley: New York, 1986. (c) Szabo, A.; Ostlund, N. S. *Modern Quantum Chemistry*; Macmillan: New York, 1982.

Table III. Stabilization Energies for **3–5**[a]

			$E^{m,n}_{stab}$,[b] kcal/mol					
compd	m	n	UHF/6-31G*	UHF/6-311G**	MP2(FC)/ 6-311G**	MP3(FC)/ 6-311G**	MP4(FC)/ 6-311G**	MP2/6-311G**
3a	2	0	4.0	2.3	2.5	2.3	**2.5**	2.6
3b	1	1	3.6	2.1	2.5	2.5	**2.7**	2.6
3c	0	2	8.0	7.5	8.5	8.0	**8.5**	8.5
4a	2	1	10.9	6.4	8.3	7.9	**8.4**	8.4
4b	1	2	15.3	12.0	14.2	13.9	**14.5**	14.4
5	2	2	21.5	13.9	17.8	17.7	**18.1**	17.9

[a] All structures optimized at the UHF/6-31G* level. [b] Stabilization energy as defined in eq 1 of the text.

observed the same effect in fluorophosphines and fluorophosphonium ions. They argued that this phenomenon is caused by "the cumulative electrostatic effect of charge withdrawal from the [central atom] to the fluorines". These results add the open-shell phosphoranyl analogues to their data.[23] While they additionally noted a tendency for the F–A–F bond angles to widen with increasing fluorine substitution, no such trend is apparent here. Schleyer and Reed proposed that angle widening in the closed-shell species improves hyperconjugation and that this effect is somewhat larger than the competing tendency for A–F bond hybrids to develop more p character with increasing fluorine substitution, which would tend to decrease F–A–F bond angles. While we do note hyperconjugative effects in the phosphoranyl series (vide infra), the presence of two pairs of unique bond types, apical and equatorial, apparently introduces a perturbation that tends to mask any effect on bond angles.

Finally, Table I reveals a curious dichotomy in energies of "axialization". Thus, the energy difference between **2a** and **2b** is about that between **3a** and **3b**, roughly 9.2 kcal/mol. However, a difference of only ~3.2 kcal/mol is observed between isomers **3b** and **3c** and **4a** and **4b**. Each of these isomeric pairs is related by the exchange of an axial fluorine with an equatorial proton. Figure 2 portrays the energy parallelogram one obtains by plotting relative energies against the number of axial fluorine atoms.

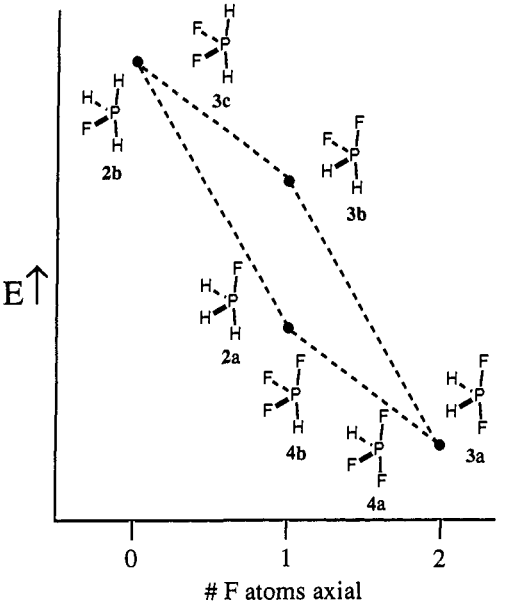

Figure 2. Relative energy vs number of axial fluorine atoms for **2–4** at the UMP4/6-311G**//UHF/6-31G* level. No comparison of energies except within an isomeric series is intended. The dotted lines illustrate the symmetrical relationships between the energy differences for certain isomers.

Discussion

Relative and Absolute Equilibrium Stabilities. In order to quantitatively assess hyperconjugative effects involving multiple fluorine atoms, we have employed the isodesmic eq 1, which

$$E[F_m{}^aF_n{}^ePH_{(4-m-n)}] + (m + n - 1)E[PH_4] = mE[F^aPH_3] + nE[F^ePH_3] - E^{m,n}{}_{stab} \quad (1)$$

expresses the stabilization energy for the polyfluorinated compounds relative to the monofluorinated. This equation is a slightly modified form of the one used by Schleyer and Reed[22] and recognizes the inherent differences between apical ($P–F^a$) and equatorial ($P–F^e$) phosphorus–fluorine bonds.[24] A positive E_{stab} implies net stabilization of the polyfluorophosphoranyl through fluorine–fluorine interaction. This sign convention is chosen so that the equivalent ΔE for the process implied in eq 1 expressed as a chemical equilibrium will be of identical sign.

The stabilization energies at various levels of theory are collected in Table III for compounds **3–5**. In general, E_{stab} tends to be seriously overestimated at the UHF/6-31G* level. This is not the case for **3c**, however. It may thus be that adequate treatment of hyperconjugative effects requires the valence-triple-ζ basis set only for those phosphoranyls having an axial P–F bond. As observed for the closed-shell species,[22] inclusion of correlation effects results in a marked increase in E_{stab}. However, correlation beyond the UMP2 level results in comparatively little change.

One is immediately struck by the very small stabilization energies for axial–axial (aa) and axial–equatorial (ae) interactions relative to equatorial–equatorial (ee). Thus, for **3a** and **3b**, E_{stab} is a mere 2.5 and 2.7 kcal/mol, respectively, while for **3c** it is a respectable 8.5 kcal/mol.[25] This effect remains in **4**, where E_{stab} for **4b** (aee) is 6.1 kcal/mol larger than that for **4a** (aae), which has no ee interaction. Finally, the mere 3.6 kcal/mol increase in E_{stab} for **5** over **4b** reflects that the additional interactions present in the former compared to the latter all involve an axial fluorine atom and are thus small.

The lack of significant anomeric-type interactions between axial fluorine atoms is not very surprising. The very large $F^a–P–F^a$ bond angles afford little opportunity for overlap of fluorine lone-pair orbitals with appropriate $P–F^a$ acceptor orbitals. The same lack in the case of ae interactions is less readily explained and is probably the product of several contributing factors. First, in terms of F^e lone-pair delocalization into the apical bond system, it must be recognized that in the three-center four-electron orbital subsystem that the $X^a–P–X^a$ fragment gives rise to, the antibonding acceptor orbital is not of p-type symmetry; the 3c–4e *nonbonding* orbital, which *is* of correct symmetry, is filled and thus leads only to *de*stabilizing interactions. Anomeric stabilization in the opposite sense, i.e., involving delocalization of F^a lone pairs into the equatorial bond system, is minimized not only by the relatively

(22) Reed, A. E.; Schleyer, P. v. R. *J. Am. Chem. Soc.* **1987**, *109*, 7362.

(23) Mulliken population analysis gives q(P) values of 0.31, 0.76, 1.14, 1.46, and 1.70 for **1**, **2a**, **3a**, **4a**, and **5**, respectively, at the UHF/6-311G**//UHF/6-31G* level.

(24) Simple stoichiometry ensures that the number of axial and equatorial phosphorus–hydrogen bonds will be conserved as well.

(25) Unless otherwise specified, all discussion of energy differences throughout will be at the UMP4/6-311G**//UHF/6-31G* level. I thank a reviewer who suggested that while these species show negligible spin contamination, nevertheless projecting out the major s + 1 spin contaminant may have a significant effect. In fact, by the UMP4 level the projected energies (PMP4) are only ~1.0 millihartree below those from the unprojected wave function, and relative energies between isomers differ by 0.0–0.3 kcal/mol. At the UHF level the differences are slightly more profound at ca. 3.0 millihartree. Absolute and relative PUHF and PMPn energies are provided as supplementary material.

Table IV. Predicted Stabilization Energies for **4** and **5** Assuming Additivity of Hyperconjugative Interactions[a,b]

			Predicted $E^{m,n}_{stab}$, kcal/mol (error, %)					
compd	*m*	*n*	UHF/6-31G*	UHF/6-311G**	MP2(FC)/ 6-311G**	MP3(FC)/ 6-311G**	MP4(FC)/ 6-311G**	MP2/6-311G**
4a	2	1	11.2	6.5	7.5	7.3	**7.9**	7.8
			(3)	(2)	(10)	(8)	**(6)**	(7)
4b	1	2	15.2	11.7	13.5	13.5	**13.9**	13.7
			(1)	(2)	(5)	(3)	**(4)**	(5)
5	2	2	26.4	18.2	21.0	20.8	**21.8**	21.5
			(23)	(31)	(18)	(18)	**(20)**	(20)

[a] All structures optimized at the UHF/6-31G* level. [b] Assumed interaction energies are aa = $E^{2,0}_{stab}$, ae = $E^{1,1}_{stab}$, and ee = $E^{0,2}_{stab}$. See Table III for values.

long P–F^a bonds, which decrease the efficiency of overlap with P–F^e σ^*-type orbitals, but probably also by the preference for delocalization into the much lower energy SOMO, which is also localized predominantly equatorially.[26]

We note also that stabilization energies are approximately additive upon going from **3** to **4** to **5**, although less satisfactorily for the latter (Table IV). Thus, $E^{2,1}_{stab}$ for **4a**, which has two ae interactions and one aa, is 8.4 kcal/mol, while the sum of the corresponding separate stabilizations, $E^{1,1}_{stab} + E^{1,1}_{stab} + E^{2,0}_{stab}$, is 7.9 kcal/mol. A similarly close result is obtained for **4b**, and indeed the *difference* in stabilization energies between **4a** and **4b** is almost exactly reproduced. For **5** however (four ae, one aa, and one ee interactions), the summation of the separate energies overestimates $E^{2,2}_{stab}$ by 3.7 kcal/mol. This result is unsurprising given the observed P–F bond contractions upon increasing fluorine substitution. This effect tends to raise the energy of the P–F σ^*-type orbitals in **5**, and this decreases the overall stabilization potential relative to the separated interactions derived from **3**. Nevertheless, this ability to approximately predict stabilization energies for the tri- and tetrasubstituted phosphoranyl radicals may prove of some use in predicting absolute energies (with eq 1) and thermodynamic equilibria (vide infra) for systems where computation beyond the disubstituted level would be prohibitively time consuming.

We are now in a position to comment on the curious dichotomy in axialization energies illustrated in Figure 2. Defining E_{ax} according to eq 2, with a sign convention identical with eq 1, one

$$E[F^aPH_3] = E[F^ePH_3] - E_{ax} \quad (2)$$

$$\Delta E_{rxn} = \Delta E_{stab} - \Delta_{ax}E_{ax} \quad (3)$$

finds that for any equilibrium process involving **1–5**, ΔE is the difference between the change in stabilization energies (ΔE_{stab}) and net axialization energy. This is expressed in eq 3, which is derived in the Appendix, where Δ_{ax} is the change in the number of axial fluorine atoms (from left to right). Thus, the relatively smaller (equilibrium) energy differences between **3b** and **3c** or **4a** and **4b** relative to **2a** and **2b** or **3a** and **3b**, reflect the large gain in stabilization energy afforded by the new ee interactions, which arise in the former two instances but not the latter.

The tendency for ee-type stabilization to offset apicophilicity provides a fascinating insight into the potential preference for TBP_a vs TBP_e geometries in certain cases. Thus, phosphoranyls substituted with three or four substituents, which may participate in significant hyperconjugative interactions, but which are not particularly apicophilic, may maximize such ee anomeric effects by adopting TBP_a geometries. The observation that the C_{3v} symmetric, TBP_a trihydroxyphosphoranyl radical is a local minimum,[27] while the analogous monohydroxy congener is a saddle point,[11a] provides some support for this analysis.[28]

Scheme I

	ΔE_{stab}	+	$\Delta_{ax}{}^{\bullet} E_{ax}$	=	ΔE
I: $PH_4 + H_2PF_2 \rightleftharpoons 2\,H_3PF$	2.5		0.0		**2.5**
II: $PH_4 + HPF_3 \rightleftharpoons H_3PF + H_2PF_2$	5.9		-9.2		**-3.3**
III: $PH_4 + PF_4 \rightleftharpoons H_3PF + HPF_3$	9.7		-9.2		**0.5**
IV: $PH_4 + PF_4 \rightleftharpoons 2\,H_2PF_2$	13.1		-18.4		**-5.3**
V: $H_3PF + HPF_3 \rightleftharpoons 2\,H_2PF_2$	3.4		-9.2		**-5.8**
VI: $H_3PF + PF_4 \rightleftharpoons H_2PF_2 + HPF_3$	7.2		-9.2		**-2.0**
VII: $H_2PF_2 + PF_4 \rightleftharpoons 2\,HPF_3$	3.8		0.0		**3.8**

The power of eq 3 to decompose otherwise obscure equilibrium ΔE's is illustrated in Scheme I, which lists all of the possible nondegenerate equilibria involving two molecules of **1–5** as both educts and products. For simplicity, only reactions with the lowest energy isomers of **2**, **3**, and **4** are considered; however, eq 3 would apply equally well without this constraint.

In the absence of a net change in axial fluorine atoms, as in reactions I and VII, only stabilization energies determine the direction of the equilibrium. In reaction I, only **3** *has* any stabilization energy, and in reaction VII, although the educts and products both enjoy two aa and four ae interactions, only the educt **5** is afforded an ee-type interaction. The small magnitude of the net ΔE in this latter instance reflects the decreased values of the hyperconjugative interactions in **5** relative to **4a** (vide supra).

In reaction III, educt **5** may take advantage of all of the interactions available to product **4a**, plus an additional one of ee- and two of ae-type. This is sufficient to force the equilibrium slightly to the left, in spite of the net gain of one axial fluorine atom on going to the right! In the remaining instances, the net gain of one (or two in the case of reaction IV) axial fluorine atom(s) drives the equilibrium to the right.

The net stabilization afforded on going from one to two axial and one to two equatorial fluorine atoms, as illustrated in Scheme I, gives rise to a phenomenon mnemonically described as the "rule of evens". This rule asserts in general that *any equilibrium involving only minimum-energy, TBP_e phosphoranyl isomers substituted with electron-withdrawing groups that possess lone pairs will favor the side with the larger number of di- and tetrasubstituted species.* In Scheme I, the rule of evens accurately predicts the direction of equilibrium for all but reaction VI, about which it makes no statement since there are equal numbers of di- and tetrasubstituted species on each side. While the rule is probably general for any one electron-withdrawing group, in the case of multiple, different electron-withdrawing groups it is best applied with caution. In the particular case of the fluoro-

(26) Of course, this is only allowed for electrons of appropriate spin. The tendency for such delocalization to occur is manifested in the rotation coordinates for hydroxyphosphoranyls with axial hydroxyl groups. See: Reference 11a.

(27) Cramer, C. J., unpublished results.

(28) Implicit in this argument is the assumption that the ee stabilization energies also overwhelm any change in hyperconjugation energies involving the singly occupied orbital, as well as its inherent "apicophobia". The energy change associated with the latter phenomenon is certainly not trivial. See: References 4, 8, 11a, and 27.

(29) (a) Weltner, W. *Magnetic Atoms and Molecules*; Scientific and Academic Editions: New York, 1983. (b) Symons, M. *Chemical and Biochemical Aspects of Electron Spin Resonance*; John Wiley & Sons: New York, 1978. (c) Ayscough, P. B. *Electron Spin Resonance in Chemistry*; Methuen: London, 1967.

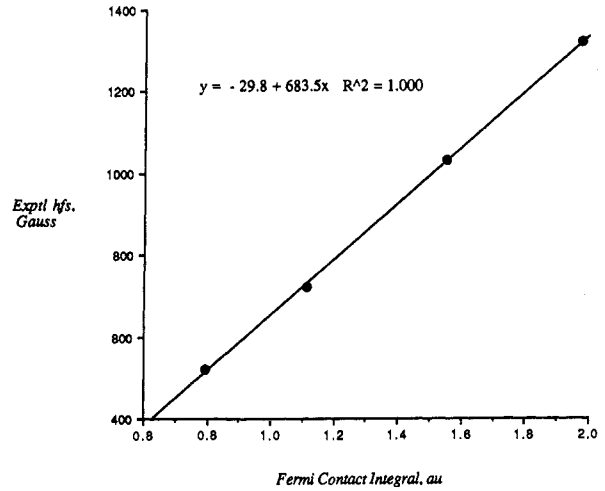

Figure 3. Calculated phosphorus Fermi contact values for **1**, **2a**, **4a**, and **5** vs experimentally measured isotropic hyperfine coupling constants. Calculations were performed for geometries optimized at the UHF/6-31G* level with the UMP2/6-311G** density matrix (see Tables V and VII).

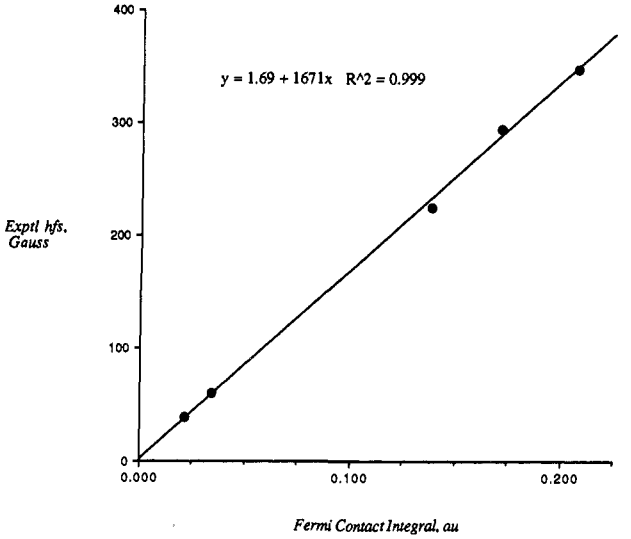

Figure 4. Calculated fluorine Fermi contact values for **1**, **2a**, **4a**, and **5** vs experimentally measured isotropic hyperfine coupling constants. Calculations were performed for geometries optimized at the UHF/6-31G* level with the UMP2/6-311G** density matrix (see Tables V and VII).

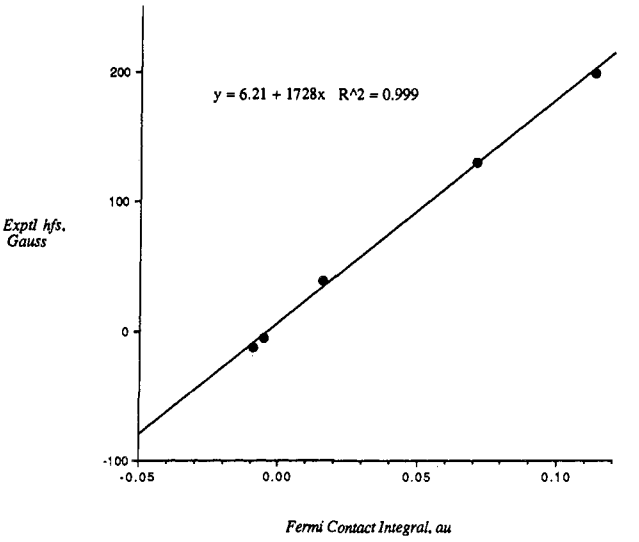

Figure 5. Calculated hydrogen Fermi contact values for **1**, **2a**, **4a**, and **5** vs experimentally measured isotropic hyperfine coupling constants. Calculations were performed for geometries optimized at the UHF/6-31G* level with the UMP2/6-311G** density matrix (see Tables V and VII).

phosphoranyls, it suggests that it should not be difficult to prepare measurable quantities of the as yet experimentally unobserved **3**, given a judicious initial stoichiometry of reactants. Additionally, these same precepts will likely hold for closed-shell phosphoranes and analogues.

Localization of Spin: Comparison to ESR Spectroscopy. Owing to their metastability, the characterization of phosphoranyl radicals has relied heavily on spectroscopic techniques, with electron spin resonance being the method of choice.[3] By analysis of hyperfine coupling to various substituent atoms, a quantitative assessment of doublet spin densities at the nuclei may be obtained with eq 4. Thus, the isotropic hyperfine coupling to any nucleus, a_N, is

$$a_N = (8\pi/3)gg_N\beta\beta_N\rho(N) \quad (4)$$

$$\rho(N) = \sum_{\mu\nu}\mathbf{P}^{\alpha-\beta}_{\mu\nu}\phi_\mu(R_N)\phi_\nu(R_N) \quad (5)$$

related to g (g_N), the electronic (nuclear) g factor, β (β_N), the Bohr (nuclear) magneton, and the Fermi contact integral, $\rho(N)$. In order to predict a_N ab initio, one need only calculate the Fermi contact integral. This calculation proceeds from the final one-electron spin density matrix according to eq 5, where the atomic basis functions, ϕ_n, are evaluated at the nuclear coordinates, R_N.[30]

Many early studies tended to discount the importance of the contribution to spin density at the nucleus from overlap of orbitals centered on other atoms and instead employed eq 6 to calculate

$$a_N = A_0(N)|\psi^2_{ns}(N)| \quad (6)$$

$$A_0(N) = (8\pi/3)gg_N\beta\beta_N|\psi^2(0)| \quad (7)$$

a_N.[31] The nucleus-dependent factor $A_0(N)$, defined in eq 7, incorporates the same constants as eq 4, together with the unperturbed, absolute spin density at the nucleus, $\psi^2(0)$, as estimated from high-level calculations on the free atom. This term may additionally be decomposed by principle quantum number. The assumption is then made that, in the vicinity of the nucleus, the pure atomic basis functions are little perturbed by bonding effects. The final term in eq 6 is the total s-orbital spin over all space. Thus, $A_0(N)$ provides an estimate of the maximum hyperfine coupling constant that could be observed for a given nucleus, i.e., $|\psi^2_{ns}(N)| = 1$. By use of this latter method, hyperfine coupling constants for **1**, **2**, **4**, and **5** have been predicted at the INDO,[7a] Hückel,[7a] and 4-31G[4] levels. Agreement with experiment is qualitative at best (vide infra).

In an attempt to improve upon these early studies, we performed additional calculations on both the UHF/6-31G* and UMP2/6-31G* optimized geometries of **1**, **2a**, **3a**, **4a**, **5**. For each of the two geometries, single-point calculations employing the polarized, valence-triple-ζ basis 6-311G** were performed at both the SCF and MP2 levels. Fermi contact values and s-orbital spin densities[32] (the latter derived from a Mulliken partitioning[33]) were calculated

(30) The ab initio prediction of hfs constants via such methodology has been assessed at many levels. (a) INDO: Pople, J. A.; Beveridge, D. L. *Approximate Molecular Orbital Theory*; McGraw-Hill: New York, 1970. (b) MNDO: Glidewell, C. *Inorg. Chim. Acta* **1984**, *83*, L81. (c) MINDO/3: Pandey, P. K. K.; Chandra, P. *Can. J. Chem.* **1979**, *57*, 3126. (d) Claxton, T. A.; Chen, T.; Symons, M. C. R.; Glidewell, C. *Faraday Discuss. Chem. Soc.* **1984**, *78*, 121. (e) Chipman, D. M. *J. Chem. Phys.* **1983**, *78*, 4785. (f) MP2: Sekino, H.; Bartlett, R. J. *J. Chem. Phys.* **1985**, *82*, 4225. CI: (g) Carmichael, I. *J. Phys. Chem.* **1987**, *91*, 6443. (h) Feller, D.; Davidson, E. R. *J. Chem. Phys.* **1984**, *80*, 1006. (i) Knight, L. B., Jr.; Steadman, J.; Feller, D.; Davidson, E. R. *J. Am. Chem. Soc.* **1984**, *106*, 3700. (j) Nakatsuji, H.; Izawa, M. *J. Chem. Phys.* **1989**, *91*, 6205.

(31) (a) Hurd, C. M.; Coodin, P. *J. Phys. Chem. Solids* **1967**, *28*, 523. (b) Morton, J. R. *Chem. Rev.* **1964**, *64*, 453. (c) Clementi, E.; Roothaan, C. C. E.; Yoshimini, M. *Phys. Rev.* **1962**, *127*, 1618. See also: Reference 6.

(32) As the 6-311G** basis employs the five Cartesian d functions on heavy atoms, no ambiguity arises over $d_{x^2} + d_{y^2}$ contributions to s-orbital spin density.

Table V. Calculated Fermi Contact Integrals for **1**, **2a**, **3a**, **4a**, and **5**[a]

		Fermi contact integral, au				
		UHF/6-31G* geometry		UMP2/6-31G* geometry		
compd	atom type	UHF density	UMP2 density	UHF density	UMP2 density	exptl hfs.[b] G
1	P	0.7618	**0.7930**	0.7652	0.8010	519
	H^{ax}	0.1207	**0.1127**	0.1238	0.1150	199
	H^{eq}	−0.0110	**−0.0056**	−0.0113	−0.0057	−6
2a	P	1.2125	**1.1134**	1.2601	1.1606	721
	F	0.2466	**0.2070**	0.2517	0.2085	347
	H^{ax}	0.0783	**0.0709**	0.0793	0.0714	130.1
	H^{eq}	−0.0154	**−0.0095**	−0.0155	−0.0093	−12.6
3a	P	1.5239	**1.3315**	1.5826	1.3863	
	F	0.1621	**0.1246**	0.1637	0.1249	
	H	−0.0050	**0.0001**	−0.0048	0.0005	
4a	P	1.7099	**1.5489**	1.7794	1.6150	1031
	F^{ax}	0.1730	**0.1382**	0.1739	0.1371	225.2
	F^{eq}	0.0222	**0.0215**	0.0208	0.0208	38.5
	H	0.0111	**0.0155**	0.0114	0.0161	38.5
5	P	2.0806	**1.9755**	2.1690	2.0725	1322
	F^{ax}	0.2018	**0.1712**	0.2010	0.1680	294
	F^{eq}	0.0288	**0.0342**	0.0265	0.0324	59.5

[a] UHF and UMP2 densities obtained with the 6-311G** basis set. [b] Taken from ref 7a.

Table VI. Calculated Total s-Orbital Spin for **1**, **2a**, **3a**, **4a**, and **5**[a]

		total s-orbital spin, au				
		UHF/6-31G* geometry		UMP2/6-31G* geometry		
compd	atom type	UHF density	UMP2 density	UHF density	UMP2 density	exptl hfs.[b] G
1	P	0.0733	0.0751	0.0712	0.0739	519
	H^{ax}	0.3991	0.3660	0.4108	0.4486	199
	H^{eq}	−0.0372	−0.0319	−0.0505	−0.0316	−6
2a	P	0.2196	0.1988	0.2171	0.1975	721
	F	−0.0096	−0.0099	−0.0110	−0.0098	347
	H^{ax}	0.2298	0.1975	0.2353	0.2014	130.1
	H^{eq}	−0.0564	−0.0370	−0.0567	−0.0363	−12.6
3a	P	0.2934	0.2903	0.2614	0.2590	
	F	−0.0050	−0.0049	−0.0048	−0.0047	
	H	−0.0312	−0.0298	−0.0157	−0.0138	
4a	P	0.3295	0.3244	0.3127	0.3076	1031
	F^{ax}	−0.0062	−0.0059	−0.0065	−0.0062	225.2
	F^{eq}	−0.0005	−0.0005	−0.0006	−0.0005	38.5
	H	0.0149	0.0174	0.0261	0.0295	38.5
5	P	0.3949	0.3886	0.4000	0.3940	1322
	F^{ax}	−0.0075	−0.0072	−0.0085	−0.0081	294
	F^{eq}	−0.0012	−0.0012	−0.0020	−0.0018	59.5

[a] UHF and UMP2 densities obtained with the 6-311G** basis set. [b] Taken from ref 7a.

from the SCF and the Z-vector-derived[18] UMP2 density matrices. The resulting data are compiled in Tables V and VI. It is noteworthy that significant differences (up to 50%!) are found between the SCF and UMP2 data.

Ignoring for the moment the question of absolute error magnitudes, we will first focus on the question of whether error within the fluorophosphoranyl series is statistically random, or is well conserved. A simple measure of this is the correlation constant, R^2, obtained from plotting a_N vs the theoretical data for any one method. Thus, the experimental a_N are plotted against the Fermi contact values obtained from the UMP2/6-311G** electron density at the UHF/6-31G* geometry in Figures 3–5 for phosphorus, fluorine, and hydrogen, respectively. While linear correlation coefficients derived from four or five points must be interpreted with caution, the predicted data for all three atoms exhibit a remarkably high correlation with experiment. The linear regression data from each of the four analyses (two spin density matrices, two geometries) are summarized in Table VII for Fermi contact values and Table VIII for s-orbital spin densities. The latter includes the lower level computations mentioned above.

It is true in nearly every case that the correlation of experiment with data obtained from the UMP2 density is improved over that from the SCF density. There is not, however, so obvious a preference for evaluating that density at the UMP2 geometry compared to the SCF. Indeed, given the very large time investment required to perform UMP2/6-31G* geometry optimizations, the equivocal nature of the resulting data tends to mitigate against such a step.

As to the choice of employing the methodology implicit in eq 4 relative to eq 6, it is evident that the former does represent an

Table VII. Linear Regression Data by Atom, Density Method, and Geometry for Fermi Contact Integrals vs Experimental hfs[a]

nucleus	density matrix[b]	geom optimized[c]	regressn slope, G/au	regressn intercept, G	corr const. R^2
^{31}P	UHF	UHF	607.9	22.1	0.987
	UMP2	**UHF**	**683.5**	**−29.8**	**1.000**
	UHF	UMP2	571.5	44.7	0.985
	UMP2	UMP2	638.0	−2.77	0.999
^{19}F	UHF	UHF	1340	12.6	0.992
	UMP2	**UHF**	**1671**	**1.69**	**0.999**
	UHF	UMP2	1310	16.3	0.991
	UMP2	UMP2	1661	4.57	0.998
^{1}H	UHF	UHF	1529	13.6	0.997
	UMP2	**UHF**	**1728**	**6.21**	**0.999**
	UHF	UMP2	1497	13.6	0.998
	UMP2	UMP2	1702	5.99	0.998

[a] Data for linear regressions taken from Table V. [b] Density matrices are either UHF = UHF/6-311G** or UMP2 = UMP2/6-311G**. [c] Geometries optimized at either the UHF = UHF/6-31G* or UMP2 = UMP2/6-31G* levels.

(33) Although other techniques purporting to give electron density distributions improved over Mulliken population analysis have appeared, the great speed with which the latter may be accomplished still makes it an attractive method.

Table VIII. Linear Regression Data by Atom, Density Method, and Geometry for Total s-Orbital Spin vs Experimental hfs[a]

nucleus	density matrix[b]	geom optimized[c]	regressn slope, G/au	regressn intercept, G	corr const, R^2
^{31}P	UHF	UHF	2431	280	0.942
	UMP2	UHF	2446	286	0.956
	UHF	UMP2	2487	285	0.962
	UMP2	UMP2	2512	287	0.976
	INDO[d]	INDO[d]	−5695	1820	0.098
	Hückel[d]	INDO[d]	5281	−821	0.994
	4-31G[e]	4-31G[e]	3238	278	0.944[f]
^{19}F	UHF	UHF	−3466	19.6	0.996
	UMP2	UHF	−3156	12.3	0.991
	UHF	UMP2	−3433	23.3	0.989
	UMP2	UMP2	−3449	10.8	0.996
	INDO[d]	INDO[d]	26120	82.8	0.786
	Hückel[d]	INDO[d]	13520	36.8	0.918
	4-31G[e]	4-31G[e]	8886	142	0.124
^{1}H	UHF	UHF	463.2	18.8	0.991
	UMP2	UHF	449.5	19.0	0.995
	UHF	UMP2	520.4	16.5	0.986
	UMP2	UMP2	438.2	16.2	0.965
	INDO[d]	INDO[d]	374.0	23.6	0.677
	Hückel[d]	INDO[d]	649.1	7.07	0.708
	4-31G[e]	4-31G[e]	334.3	26.8	0.966[f]

[a] Data for linear regressions taken from Table VI unless otherwise indicated. [b] Density matrices are either INDO, Hückel, 4-31G = UHF/4-31G, UHF = UHF/6-311G**, or UMP2 = UMP2/6-311G**. [c] Geometries optimized at either the INDO, 4-31G = UHF/4-31G, UHF = UHF/6-31G*, or UMP2 = UMP2/6-31G* levels. [d] Data taken from ref 7a. [e] Data taken from ref 4. [f] Regression is on only three data points.

improvement over the latter, with the most marked effect being at phosphorus. However, the difference between the two methods is meager enough that the lower correlations exhibited at the INDO, Hückel, and 4-31G levels are more an indictment of the low level of theory than the technique, at least in this instance.

Turning now to the issue of absolute predictive capabilities, it is evident from eq 4 that if calculation matches theory exactly, the slopes in Table VII should be the product of the electronic and nuclear constants. These constants are 646, 1430, and 1600 G/au for phosphorus, fluorine, and hydrogen, respectively.[29] The intercepts should, of course, be zero. From inspection of Table VII, it appears that again the UMP2 density methods do better where zeroing the intercept is concerned, but the results are equivocal with respect to slope. The uniformly larger slopes relative to the expected constants indicates that even at this high level, the Fermi contact integrals are underestimating the total spin at the nucleus. However, if this underestimation is consistent across a range of molecules, modification of eq 4 by addition of another constant factor, G_N^{basis}, which depends on both basis set and atom,[34] would make these results particularly useful.

A similar analysis applies to eq 6 and Table VIII. Here the theoretical values of A_0 are 3636, 17110, and 508 G/au for phosphorus, fluorine, and hydrogen, respectively,[29] and again the intercepts are expected to be zero. It is immediately evident, however, that although a reasonable correlation exists between experimental data and predicted s-orbital spin density, it does not follow closely the form of eq 6. This seems to suggest that the use of A_0(N), which relies on information calculated from the wave function for the free atom, may not be sufficient in analysis of molecular spin density distribution. We are not yet in a position to offer a theoretical underpinning for our here empirically derived constants.

Noting the excellent correlations between theory and experiment, we feel confident that hfs constants for the as yet unobserved **3a** may be predicted with great accuracy. Employing Fermi contact values calculated from the UMP2/6-311G** density at the UHF/6-31G* geometry (Table VII), we predict from our regression data a_P = 880 G, a_F = 210 G, and a_H = 6 G.

The trend for a_P to increase in this series with increasing fluorine substitution is a final phenomenon worthy of note. This behavior, which has also been noted in DT phosphoranyl radicals with general substituents of increasing electronegativity,[2a] is entirely consistent with expected phosphorus orbital rehybridizations; i.e., increasing p character in the bonding to fluorine with concomitantly increasing s character afforded the SOMO. The similar but less regular trends observed for fluorine and hydrogen reflect not only orbital rehybridization, but also the progressively shortening bonds.

Conclusion

Although the fluorophosphoranyl series is similar to its closed-shell, tricoordinate analogues in exhibiting bond contraction with increasing fluorine substitution, it manifests significantly different hyperconjugative interactions as a result of the TBP_e geometry unique to the open-shell, tetracoordinate species. Thus, stabilizing interactions between two equatorially disposed fluorine atoms are considerably greater than any involving one or more axial fluorine atoms. Such stabilization effects are approximately additive within the series. The energy change for any reaction involving fluorine metathesis and/or isomerization within the series may be decomposed into separate terms describing the hyperconjugative changes and the net gain or loss of axially disposed fluorine atoms. The combination of these effects is such that, when only the minimum-energy isomers are considered, equilibrium will always favor the side having more di- or tetrasubstituted species. These observations are expected to be general for electronegative substituents and may perhaps apply analogously to the pentacoordinate phosphoranes.

In addition, whereas lower level computations on this series have fared poorly in predicting isotropic hyperfine coupling constants from s-orbital spin density, employment of Fermi contact values derived from UMP2 electron densities gives excellent correlation with experiment: some scaling of the predicted a_N is required, much as with theoretically predicted infrared spectra.[34,35] Given the relative ease of these computations, the possibility that such accuracy may be conserved in and across unrelated systems is an exciting one, the aspects of which are the subject of current investigation.

Acknowledgment. Funding for this work was provided under projects 1C162622A553I and 1L161102A71A. I am grateful to John Holter and Linda Stine for hardware technical assistance.

Appendix

The ΔE for the general reaction of any two phosphoranyls in the series **1–5**, formally a hydrogen–fluorine metathesis process, may be derived from eq i. Stoichiometry constraints give rise

$$E[F_m{}^aF_n{}^eP_{(4-m-n)}] + E[F_j{}^aF_k{}^eP_{(4-j-k)}] = E[F_{m'}{}^aF_{n'}{}^eP_{(4-m'-n')}] + E[F_{j'}{}^aF_{k'}{}^eP_{(4-j'-k')}] - \Delta E_{rxn} \quad \text{(i)}$$

$$m + n + j + k = m' + n' + j' + k' \quad \text{(ii)}$$

to eq ii. Substituting for each individual energy term in eq i by using a slightly rearranged form of eq 1 from the text affords eq iii. Rearrangement and collection of like terms leads to eq iv.

$$mE[F^aPH_3] + nE[F^ePH_3] - (m + n - 1)E[PH_4] - E_{stab}{}^{m,n} + jE[F^aPH_3] + kE[F^ePH_3] - (j + k - 1)E[PH_4] - E_{stab}{}^{j,k} = m'E[F^aPH_3] + n'E[F^ePH_3] - (m' + n' - 1)E[PH_4] - E_{stab}{}^{m',n'} + j'E[F^aPH_3] + k'E[F^ePH_3] - (j' + k' - 1)E[PH_4] - E_{stab}{}^{j',k'} - \Delta E_{rxn} \quad \text{(iii)}$$

$$\Delta E_{rxn} = \Delta E_{stab} + (m + n + j + k - m' - n' - j' - k')E[PH_4] + (m' + j' - m - j)E[F^aPH_3] + (n' + k' - n - k)E[F^ePH_3] \quad \text{(iv)}$$

(34) From these results with the 6-311G** basis set, $G_P \approx 1.06$, $G_F \approx 1.17$, and $G_H \approx 1.08$. The roughly 10% underestimations at this level have been observed in a number of other instances for both these and other atoms: Cramer, C. J., unpublished results.

(35) There is a certain pleasing symmetry in noting that the degree to which hyperfine couplings are *under*estimated is about the same as that to which infrared absorptions are *over*estimated. (For a discussion of ab initio prediction of infrared spectra, see ref 21b.)

where $\Delta E_{stab} = E_{stab}^{m,n} + E_{stab}^{j,k} - E_{stab}^{m',n'} - E_{stab}^{j',k'}$, i.e., the net change in stabilization energy on going from educts to products.

Now, noting by the application of eq ii that the coefficient of the term involving $E[PH_4]$ in eq iv is zero, and using eq 2 of the text to substitute for $E[F^ePH_3]$, we may derive after collection of like terms eq v. Here eq ii may again be applied, now eliminating the term involving $E[F^ePH_3]$, which delivers the desired eq 3, where $\Delta_{ax} = m' + j' - m - j$, i.e. the net change in the number of axial fluorine atoms on going from left to right.

$$\Delta E_{rxn} = \Delta E_{stab} + (m + j' - m - j + n' + k' - n - k)E[F^ePH_3] - (m' + j' - m - j)E_{ax} \quad (v)$$

$$\Delta E_{rxn} = \Delta E_{stab} - \Delta_{ax}E_{ax}$$

Although derived from the bimolecular case, eq 3 obviously holds for metatheses of termolecular and higher order as well. However, the likelihood of such reactions is minimal.

Note Added in Proof. Observation of axial-equatorial differences in anomeric stabilization has recently been made for closed-shell TBP systems as predicted here. See: Wang, P.; Zhang, Y.; Glaser, R.; Reed, A. E.; Schleyer, P. v. R.; Streitwieser, A. *J. Am. Chem. Soc.* **1991**, *113*, 55.

Supplementary Material Available: Table of absolute and relative projected UHF and PMPn energies for **1-5** (1 page). Ordering information is given on any current masthead page.

Correlation of Carbon-13 and Oxygen-17 Chemical Shifts and the Vibrational Frequency of Electrically Perturbed Carbon Monoxide: A Possible Model for Distal Ligand Effects in Carbonmonoxyheme Proteins

Joseph D. Augspurger,† Clifford E. Dykstra,* and Eric Oldfield

Contribution from the Department of Chemistry, University of Illinois, Urbana, Illinois 61801.
Received June 21, 1990

Abstract: Ab initio calculations have been carried out that demonstrate an essentially linear correlation between the vibrational frequency of carbon monoxide and its carbon-13 and oxygen-17 chemical shifts, under a variety of external electrical influences. However, the correlations for carbon-13 and oxygen-17 shifts turn out be in opposite directions. Electronic structure calculations reveal that it is polarization of the electron charge density along the intermolecular axis that changes the chemical shielding oppositely for the carbon and oxygen nuclei. Recent experiments have pointed to just such a correlation in a wide range of carbonmonoxyheme proteins, and so electrical perturbation is a possible cause of distal ligand effects. Furthermore, the experimentally determined correlation of the vibrational frequency with oxygen-17 quadrupole coupling constants is also seen in the calculations.

Introduction

Chemical shifts, nuclear quadrupole coupling constants, and vibrational frequencies have long been useful measurements for ascertaining structure and bonding. This is particularly so for complex systems with embedded submolecules, e.g., ligands. For instance, the vibrational frequency of a carbonyl in a transition metal complex (an embedded CO) and/or its chemical shift are frequently taken to be a manifestation of the nature of the metal-carbonyl bonding, with stronger bonding associated qualitatively with a greater change in the CO characteristics. A composite picture of vibrational and chemical shifts, and perhaps other data, offers the possibility of quantitative relationships with structure and interaction energetics; however, this will require knowing the detailed nature of the interactions.

In recent NMR studies of ligand interactions in heme proteins, Park and co-workers[1] established a linear relationship between carbon-13 (^{13}C) and oxygen-17 (^{17}O) chemical shifts, and the ^{17}O nuclear quadrupole coupling constant, with the CO vibrational frequency, by surveying a number of different proteins containing distal ligands which might be expected to influence the heme protein's Fe-CO in different ways. The basis for that relationship lies in the nature of the interaction, and a model of the interaction must be able to reproduce it. As a first step toward a detailed, quantitative model, we report here a theoretical correlation of chemical shifts and coupling constants with vibrational frequencies of isolated CO upon varying an external electrical perturbation in a manner not dissimilar, we believe, to that of distal ligand species in heme proteins.[1]

External electrical perturbation is a simple means of influencing molecular vibration and other properties. In the hypothetical case of a nonrotating diatomic molecule with a dipole moment function that grows linearly with the bond distance, r, a uniform, axial electric field will generate a perturbation to the stretching potential that is also a linear function of r. As a result, the perturbed stretching potential has a different equilibrium point, and this corresponds to the molecule's net contraction or extension in response to the electric field. This change is the vibrational equivalent of the pure electronic structure response to an applied field, and it may be termed vibrational polarization.[2] If the original potential is anharmonic, there will also be a change in the vibrational level spacing,[2,3] and that is observed as a shift in the vibrational transition frequency. Or, if the dipole moment function has a quadratic or higher order dependence on r, this "electrical anharmonicity"[3] will give rise to a frequency shift as well.

Polarization of the electronic charge cloud by an applied field may lead to changes in molecular properties. An obvious example is the property change identified as an induced dipole moment. The polarization of the charge density can, in principle, alter the

† University of Illinois Graduate Fellow, 1986-1990.

(1) Park, K. D.; Guo, K.; Adebodun, F.; Chiu, M. L.; Sligar, S. G.; Oldfield, E. *Biochemistry*, in press.
(2) Dykstra, C. E. *J. Chem. Educ.* **1988**, *65*, 198.
(3) DiPaolo, T.; Bouderon, C.; Sandorfy, C. *Can. J. Chem.* **1972**, *50*, 3161.

0002-7863/91/1513-2447$02.50/0